Desalination and Water Treatment
www.deswater.com

doi: 10.1080/19443994.2016.1190109

57 (2016) 26718–26729
November

Taylor & Francis
Taylor & Francis Group

Membrane distillation of high salinity wastewater from shale gas extraction: effect of antiscalants

Hyeongrak Cho[a], Yongjun Choi[a], Sangho Lee[a,*], Jinsik Sohn[a], Jaewuk Koo[b]

[a]*School of Civil and Environmental Engineering, Kookmin University, 77 Jeongneung-ro, Seongbuk-gu, Seoul, 02707, Korea, Tel. +82 2 910 4529; Fax: +82 2 910 4939; email: sanghlee@kookmin.ac.kr (S. Lee)*

[b]*Korea Institute of Civil Engineering and Building Technology, 283, Goyang-daero, Ilsanseo-gu, Goyang-si, Gyeonggi-do 10223, Republic of Korea*

Received 18 December 2015; Accepted 29 December 2015

ABSTRACT

Although shale gas has become an important source of natural gas, it has problems associated with water pollution by producing high salinity wastewater (i.e. TDS > 100,000 mg/L). Membrane distillation (MD) can be applied to treat such wastewater but may suffer from fouling due to scale formation. Accordingly, this study focused on the use of antiscalants to retard scale formation in MD process for the treatment of high salinity wastewater. Experiments were performed using a laboratory-scale direct contact MD (DCMD) system. Seven different antiscalants were applied to the simplified synthetic wastewater. The results were analyzed using a simple theoretical model. It was found that the abilities to retard scale formation were different for different antiscalants. The difference in chemical structures of the antiscalants was attributed to the changes in their effect on scale prevention. Moreover, the mechanisms of flux decline seem to be different in the presence of antiscalants. Not only surface blockage but also internal pore blocking occurred during the MD operation, and the dominant fouling mechanism changed by the addition of the antiscalants.

Keywords: Membrane distillation; Flat sheep membrane; Shale gas; Flowback water; Produced water; Scale formation

1. Introduction

Recently, shale gas has become increasingly important as a viable alternative to conventional gas resources. The production of shale gas has been enabled by the development of horizontal drilling and hydraulic fracturing technologies. The USEIA estimated that annual shale gas production in the United States will increase from 5.0 TCF (trillion cubic feet) in 2010 to 13.6 TCF in 2035 [1,2]. Not only the United States but also other countries such as China and Australia are developing shale gas resources.

However, one of the critical issues in the development of shale gas is the water contamination by the generation of wastewater. During the hydraulic fracturing, a huge quantity of wastewater is produced, including flowback and produced water. In particular,

*Corresponding author.

Presented at the 8th International Desalination Workshop (IDW) 2015, 18–21 November 2015, Jeju Island, Korea

produced water may contain high concentration of ionic compounds, which is over 100,000 mg/L. Reverse osmosis, although it is a standard technology for desalination, cannot be applied to treat such wastewater due to its high osmotic pressure (over 65 bar). Novel technologies have been suggested and evaluated for the treatment of shale gas wastewater [3], including multieffect distillation, mechanical vapor compression, forward osmosis [4,5], and membrane distillation (MD).

Among such treatment options, MD is particularly promising due to its ability to treat feed water with high salinity [6]. MD is a thermally driven separation technology using hydrophobic membranes [7]. MD possesses many advantages over other desalination technologies [8]: minimum use of electrical energy, operation under relatively low-pressure conditions, capability of using low grade heat such as waste heat and solar heat, small footprint, and low fouling propensity [9]. In theory, complete separation of the high-quality freshwater production is possible (ions, polymers, colloids, etc.) [6,10].

However, fouling of the membrane is also an issue in MD [9]. When the wastewater containing high concentration of salt is treated, the solubility limits of salt in the feed water exceed saturation levels leading to crystallization on membrane surfaces. The surface blockage of the scale results in permeate flux decline, reducing the efficiency of the process, and increasing operation costs [11]. Accordingly, it is important to overcome the problem of MD fouling due to scale formation during the treatment of shale gas wastewater.

There are some methods of scale control such as acidification, ion exchange softening, and antiscalant addiction [11–13]. In particular, antiscalants are surface active materials that interfere with precipitation reactions. First, dispersion is the ability of some antiscalants to adsorb on crystals or colloidal particles and impart a high anionic charge, which tends to keep the crystals separated. Second, crystal modification is the property of an antiscalants to distort crystal shapes, resulting in soft nonadherent scale [12,14,15]. As a crystal begin to form at the submicroscopic level, negative groups located on the antiscalant molecule attack the positive charges on scale nuclei interrupting the electronic balance necessary to propagate the crystal growth. When treated with crystal modifiers, scale crystals appear distorted, generally more oval in shape and less compact. Finally, threshold inhibition is the ability of an antiscalant to keep supersaturated solutions of soluble salt [9].

This study intended to explore the use of antiscalants to control scale formation in MD operation for the treatment of high salinity wastewater. Using a laboratory-scale direct contact MD (DCMD) system, a set of experiments was carried out. Commercially available antiscalants were added to the simplified synthetic wastewater. A simple theoretical model based on surface blockage mechanism was suggested and applied to investigate the effect of antiscalants.

2. Theory

In this study, a simple model was applied to understand the effect of antiscalants on scale prevention in MD systems [16–20]. When no fouling occurs, the flux in MD can be generally given by 6:

$$J_0 = B\Delta p \tag{1}$$

where J_0 is the water flux without fouling (kg/m^2 h); B is the MD membrane permeability (kg/m^2 h Pa); and Δp is the difference in effective vapor pressure across the MD membrane (Pa).

If scale formation occurs, the flux is reduced due to the decrease in effective membrane surface area. Accordingly, the following equation can be used:

$$J = B\Delta p(1 - \phi\beta) = J_0(1 - \phi\beta) \tag{2}$$

where ϕ is the surface blockage ratio; β is the correction factor. Here, ϕ is a crucial parameter to quantify the extent of fouling due to surface crystallization. On the other hand, β is related to the properties of the surface crystals.

The surface crystallization results in an increase in surface blockage [20]. In fact, the rate of surface crystallization is proportional to crystallization kinetics and $1-\phi$. Moreover, assuming that the changes in salt concentration during the operation are negligible, the term for the crystallization kinetics is constant. This leads to the following equation:

$$\frac{d\phi}{dt} = k_c(c - c^*)^n(1 - \phi) \approx k(1 - \phi) \tag{3}$$

where k_c is the kinetic constant for the surface crystallization; c is the salt concentration in the feed solution; c^* is the saturated concentration; n is the reaction constant; and k is the apparent kinetic constant.

The Eq. (3) is rearranged to obtain the relationship between MD operation time and the surface blockage ratio.

$$\int_0^{\phi} \frac{d\phi}{1 - \phi} = kt \tag{4}$$

$$\phi = 1 - e^{-kt} \tag{5}$$

Combining Eqs. (2) and (5), the following equation is obtained:

$$J = J_0\left(1 - \beta\left(1 - e^{-kt}\right)\right) \tag{6}$$

To determine k and β, a non-linear regression should be carried out using t and $1 - J/J_0$:

$$\left(1 - \frac{J}{J_0}\right) = \beta\left(1 - e^{-kt}\right) \tag{7}$$

3. Materials and methods

3.1. Membranes

Flat-sheet PVDF membranes (GVHP, Millipore) were used for the high-concentration feed experiments. The membrane pore size and thickness were 0.22–125 μm, respectively, and the porosity of the membrane was 75%. A laboratory-scale membrane module with an effective membrane area of 12.2 cm^2 was prepared prior to the experiments.

3.2. Experimental setup

Laboratory-scale MD system was developed and used for measuring flux and rejection in MD operation, as illustrated in Fig. 1 [21,22]. The system consisted of MD, two gear pumps, a feed tank in a water bath, flat-sheet membrane module, a condenser, an electronic balance connected to a personal computer, and a cooler. The feed conductivity and turbidity were regularly measured to confirm scale formation in process. The feed water was heated by the water bath, and the water vapor was passed through the membrane and condensed in the condenser. Sodium chloride solution of 350 g/L with the temperature of 60℃ was used as the synthetic wastewater. Gear pumps (Micro-pump, Vancouver, WA) were used to pump water. Feed side was operated in the flow rate of 400 mL/min. Permeate side was operated in the flow rate of 260 mL/min. According to our previous works, it was found that the flow rate (or flow velocity) on the permeate side does not affect the MD membrane performance. Thus, the flow rate on the permeate side was adjusted to be a reasonable value for the DCMD experiments. The permeate side was collected as an overflow and continuously monitored by an electronic balance connected to a personal computer. Table 1 shows the summary of experiment conditions.

3.3. Antiscalant

Commercially available antiscalants were added prior to the DCMD experiments. The information on the antiscalants is summarized in Table 2. A stock solution for each antiscalant (1,000 mg/L) was prepared and used for the experiments. The dosage of the antiscalant was 10 m/L.

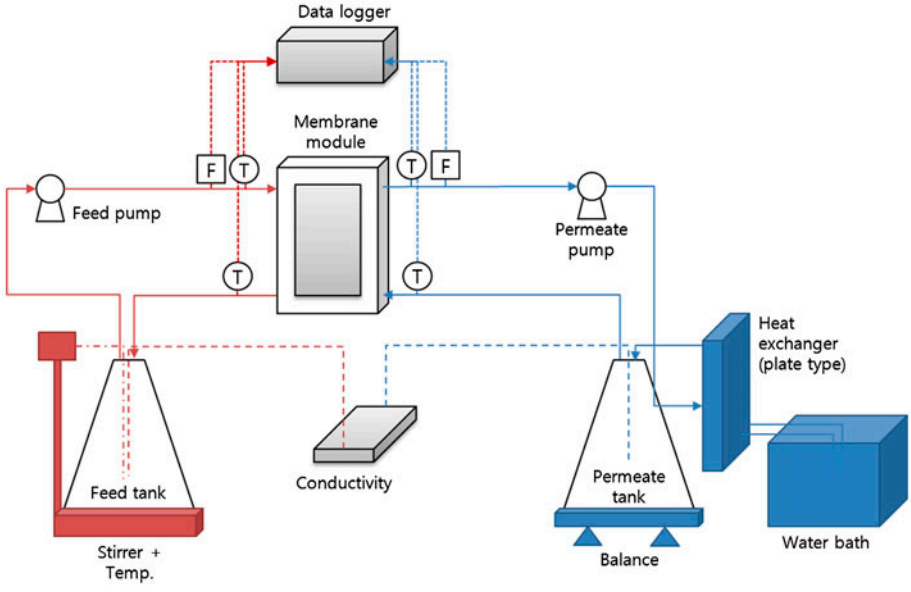

Fig. 1. Schematic diagram for a laboratory-scale DCMD system.

Table 1
Summary of experiment conditions

Item		Condition
Operation type		DCMD
Membrane		PVDF 0.22 μm
Effective membrane area		12.2 cm^2
Cross-flow velocity	Feed	0.4 L/min
	Permeate	0.26 L/min
Solution	Feed	NaCl 350 g/l
	Permeate	D.I. water
Temperature	Feed side	60°C
	Permeate side	20°C

3.4. Analytical methods

A field-enhanced scanning electron microscope (FE-SEM, Hitachi S-4700) was used to examine the membrane surface of the scale phenomena on the membrane structure after the experiments. Membrane samples were completely dried at 50°C for 12 h in a dry oven. Also, membrane samples were coated with platinum. After the experiments, the surfaces of the membranes were analyzed.

FTIR spectroscopy is a highly diverse molecular spectroscopy technique and chemical analysis method. While FTIR is frequently used for polymer testing and pharmaceutical analysis, the application of the technique is virtually limitless offering both qualitative and quantitative analyses of a wide range of organic and inorganic samples. FTIR spectrometer (Vertex, Bruker) was used for antiscalants' ingredient of organizing, and variable antiscalants were compared.

4. Results and discussions

4.1. Fouling due to scale formation in DCMD system

To begin, experiments were carried out to examine the flux decline during DCMD operation of synthetic wastewater. As shown in Fig. 2(a), the flux through the MD membrane rapidly decreases with time from the beginning. Initial water flux was 12 kg/m^2 h but the flux after 600 min was less than 0.4 kg/m^2 h. During the operation, the formation of crystals could be visually observed. It is evident that crystals formed by crystallization reduced flux through the MD membrane.

The progress of fouling by scale formation was analyzed using the Eq. (7). If the recovery of the distillate is high, the Eq. (7) cannot be used because the salt concentration (c) changes with time. However, the recovery rate of 10 h in most of the experiments was only 3%, and thus, $k_c(c - c^*)^n$ can be assumed to be constant. The correlation between $1 - J/J_0$ and time (t) was obtained using the nonlinear regression technique. The apparent rate constant (k) and correction factor (β) were determined to be 0.0166 m^{-1} and 0.897, respectively. This implies that the flux decreased to 50% of initial flux within 49 min (= –ln(1 – 0.5/0.897)/0.0166). The salt rejection was measured before and after the MD operation. Although the flux was significantly reduced, the salt rejection was maintained above 99.9%, indicating there was no pore wetting associated with scale formation.

4.2. Effect of antiscalant addition on scale formation in DCMD system

To alleviate fouling due to scale formation, antiscalants were added to the synthetic wastewater for MD operation. It should be noted that these antiscalants are not designed to be used with MD. Moreover, the salt concentration in the feed water is beyond the recommended conditions for these antiscalants. Nevertheless, the effect of antiscalants was investigated to provide insight into the development of antiscalants optimized for MD systems.

However, the flux was slightly higher than that without any antiscalant. Although the antiscalant could not completely prevent scale formation, the rate

Table 2
Summary of antiscalants

Antiscalant	Description	Manufacturer
Antiscalant A	Information not available	Nalco (PC-1850)
Antiscalant B	Blend of antiscalants and dispersants, developed specifically for high silica feed water	Nalco (PC-510T)
Antiscalant C	Phosphorous-free antiscalant	Nalco (PC-1611T)
Antiscalant D	Organophosphonate (90%) and polycarboxylic acid (~9%)	Nalco (PC-191T)
Antiscalant E	Mixture of organic phosphate and polymers	GE (MDC 220)
Antiscalant F	Mixture of organophosphonate and polycarboxylic acid	BWA water additives (Flocon 260)
Antiscalant G	Neutralized carboxylic acid (Phosphorous-free antiscalant)	Genesys (SW)

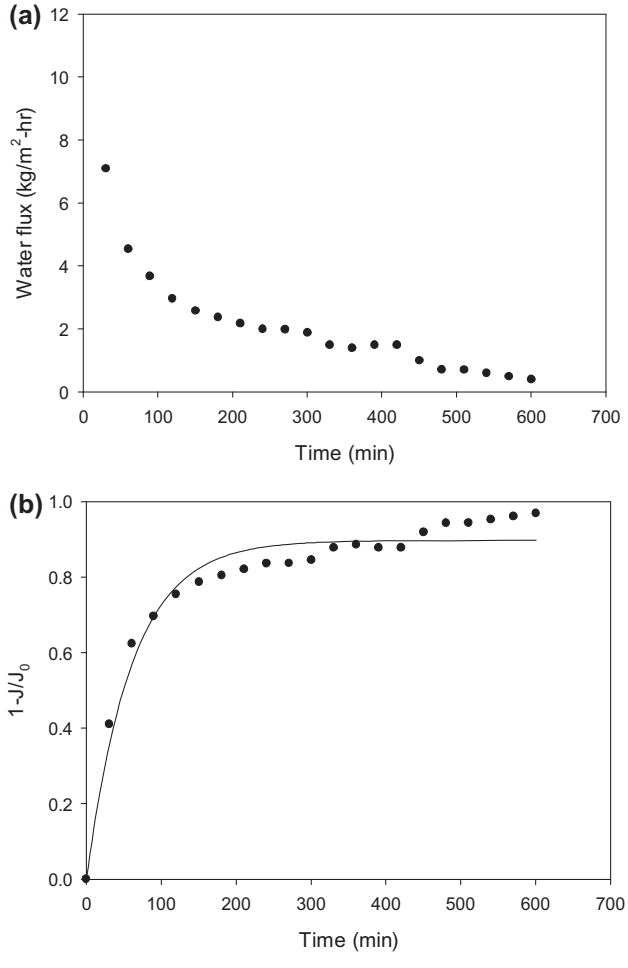

Fig. 2. Changes in flux and pore blockage ratio with time in the absence of antiscalant during DCMD operation (feed water: NaCl 350 g/L solution; feed temperature: 60℃; distillate temperature: 20℃) (a) flux and (b) pore blockage ratio (θ).

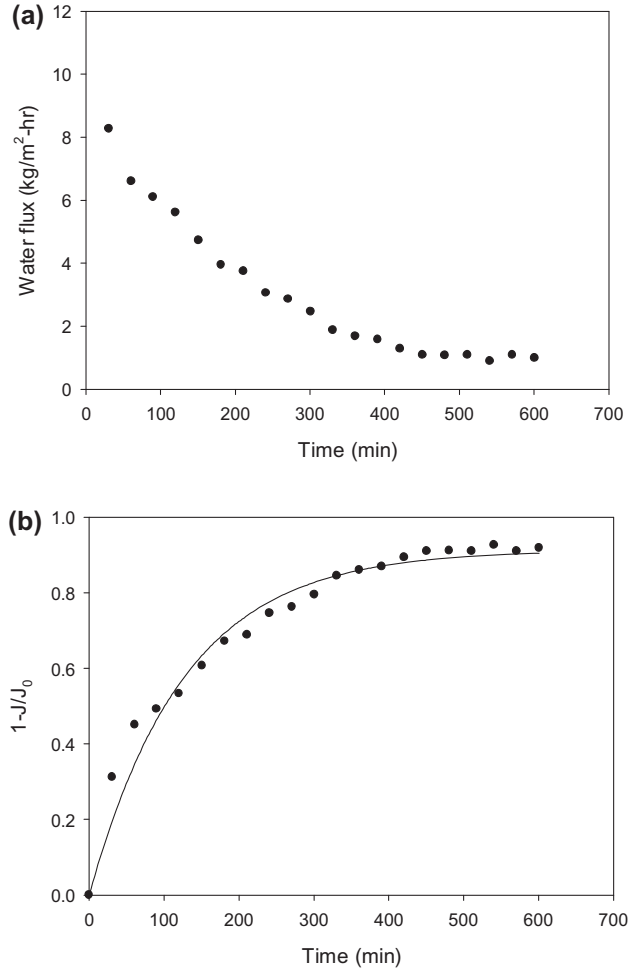

Fig. 3. Changes in flux and pore blockage ratio with time in the presence of antiscalant B during DCMD operation (feed water: NaCl 350 g/L solution; feed temperature: 60℃; distillate temperature: 20℃; antiscalant concentration: 10 mg/L) (a) flux and (b) pore blockage ratio (θ).

of scale formation seems to be lowered. In this case, the flux after 30 min was much higher (11 kg/m^2 h) than that without antiscalants (11 kg/m^2 h). This suggests that the initial flux decline was properly controlled by this antiscalant. As the time passed, the flux decreased but was still higher than that without antiscalants.

The effect of antiscalants on MD flux is important for antiscalants B, C, D, and G as shown in Figs. 3(a), 4(a), 5(a), and 6(a). In particular, the antiscalant C was found to be the most effective to increase the flux and retard the scale formation. After the addition of the antiscalant D, the initial flux was higher. Nevertheless, the final flux after 600 min was lower than the other cases.

On the other hand, the antiscalants E and F were not effective to control fouling due to scale formation, as illustrated in Figs. 7(a) and 8(a). When the antiscalant F was used, the initial flux was even lower than that without antiscalant. This is because the antiscalant F formed suspended particulate as a result of the reaction with the feed water. These particles are likely to deposit on the membrane surface from the beginning, thereby reducing the water flux. The flux profiles for all previous cases are compared in Fig. 9.

In all experiments, the recovery rate during the MD operation of 10 h ranged from 3 to 5.5%. This indicates that the changes in salt concentration during the MD operation are negligible. Nevertheless, rapid flux decline was observed within the 50 min. Since the solubility of NaCl is 360 g/L, the feed solution approaches the saturated condition. Accordingly, the scale formation seems to occur from the early stage of the MD operation.

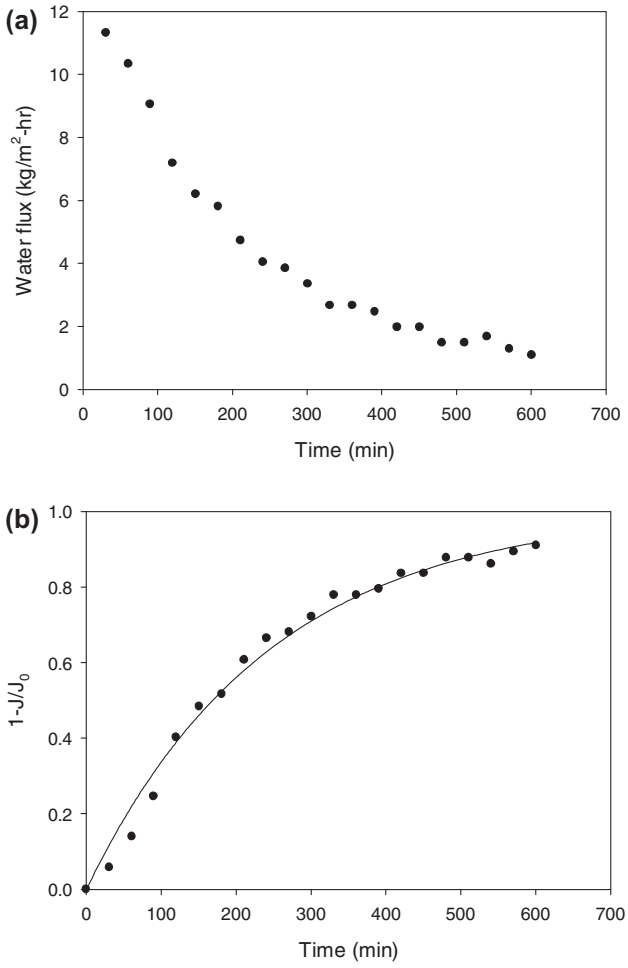

Fig. 4. Changes in flux and pore blockage ratio with time in the presence of antiscalant C during DCMD operation (feed water: NaCl 350 g/L solution; feed temperature: 60℃; distillate temperature: 20℃; antiscalant concentration: 10 mg/L) (a) flux and (b) pore blockage ratio (θ).

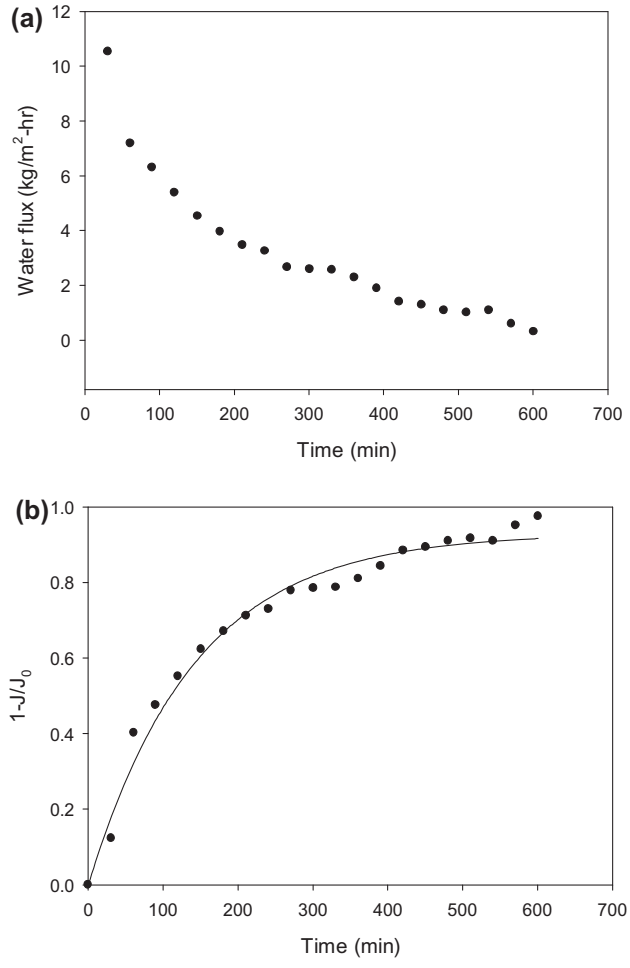

Fig. 5. Changes in flux and pore blockage ratio with time in the presence of antiscalant D during DCMD operation (feed water: NaCl 350 g/L solution; feed temperature: 60℃; distillate temperature: 20℃; antiscalant concentration: 10 mg/L) (a) flux and (b) pore blockage ratio (θ).

4.3. Quantitative estimation of the effect of antiscalants

The effectiveness of the antiscalants was compared using quantitative measures. Using the Eq. (7), the k and β were estimated. The physical meaning of k is the rate of scale formation. If an antiscalant is effective, k becomes low in the presence of the antiscalant. On the other hand, the physical meaning of β is the morphology of surface crystals. If the surface crystal layer is completely impermeable, $\beta = 1$. As the surface crystal layer becomes porous, β decreases. Since antiscalants can change the morphology of the crystals, they may affect the permeability of surface crystal layers. This is why k and β were compared for different antiscalant.

The model fits to experimental data are shown in Figs. 10(b), 3(b), 4(b), 5(b), 7(b), 8(b), and 6(b). Except for the antiscalant F, the model fits the experimental data well. The relative large deviation of the model fit from experimental data for the antiscalant F is attributed to the particle formation by the reaction of feed water and this antiscalant. Not only the surface blockage but also crystal particle deposition seems to be involved in this case, which cannot be fully predicted by the model equation.

The k values are compared in Fig. 11(a). The antiscalants B, C, D, and G resulted in low values of k while the antiscalants A, E, and F showed relatively high k values. Since k is the apparent rate constant for the scale formation, it can be concluded that the antiscalants B, C, D, and G are effective to retard scale formation. Among them, the antiscalant C was the most effective. On the other hand, the k value for the

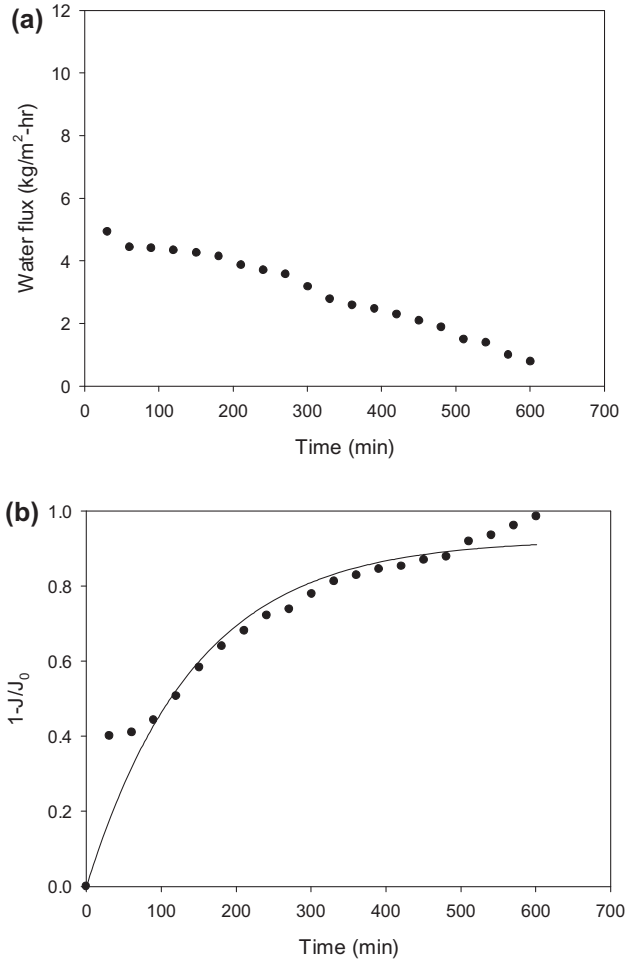

Fig. 6. Changes in flux and pore blockage ratio with time in the presence of antiscalant G during DCMD operation (feed water: NaCl 350 g/L solution; feed temperature: 60˚C; distillate temperature: 20˚C; antiscalant concentration: 10 mg/L) (a) flux and (b) pore blockage ratio (θ).

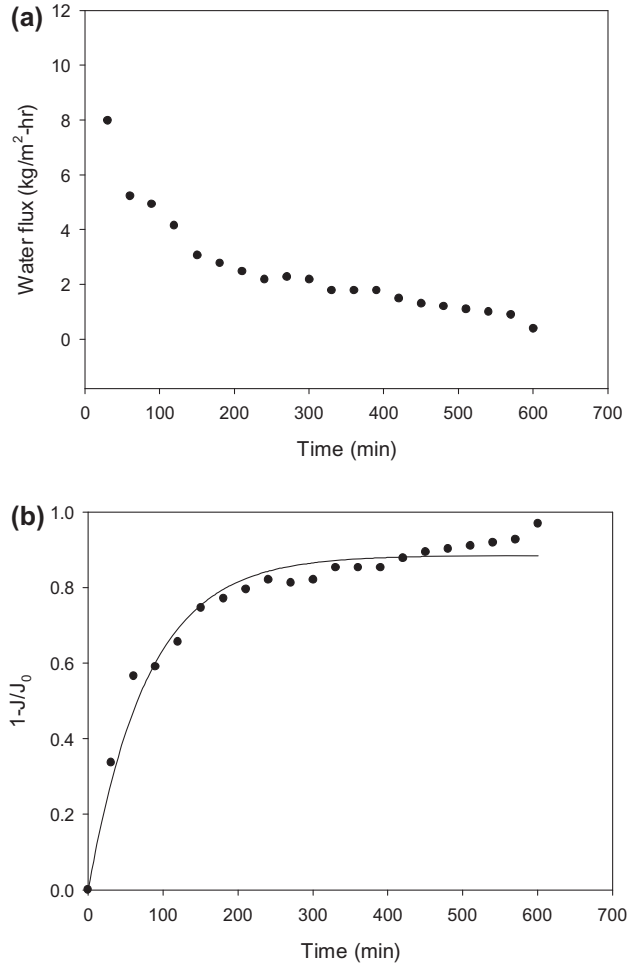

Fig. 7. Changes in flux and pore blockage ratio with time in the presence of antiscalant E during DCMD operation (feed water: NaCl 350 g/L solution; feed temperature: 60˚C; distillate temperature: 20˚C; antiscalant concentration: 10 mg/L) (a) flux and (b) pore blockage ratio (θ).

antiscalant A was similar to that without antiscalant, suggesting that this is not effective to retard scale formation.

The β values are also compared in Fig. 11(b). As previously mentioned, β is related to the properties of the surface crystal layers. If the antiscalant affects the morphology of the crystals, β is lower than one. Otherwise, β should be close to one. The results in Fig. 11(a) and (b) suggest that the mechanisms of scale control are different for different antiscalants. For instance, the antiscalant C resulted in the lowest k value but β is close to one. The antiscalants B, D, and G also showed relatively low k values, and β is about 0.9. The antiscalant A had the lowest β value but k was the highest. It appears that the antiscalant C is effective to reduce the rate of crystallization but does not affect the properties of the surface crystals. On the other hand, the antiscalants B, D, and G seem to affect both the rate of crystallization and the surface crystal properties. Moreover, the antiscalant A seems to change the properties of surface crystals without affecting the crystallization kinetics.

The effectiveness of the antiscalant can be also determined by process parameters. In Fig. 12, the relative water production and relative average flux are compared for various antiscalants. The relative water production is calculated by the total water production for 300 min with the addition of an antiscalant divided by that without antiscalant. The relative average flux is calculated by the average flux for 300 min with the addition of an antiscalant divided by that without antiscalant. If these values are higher than one, the

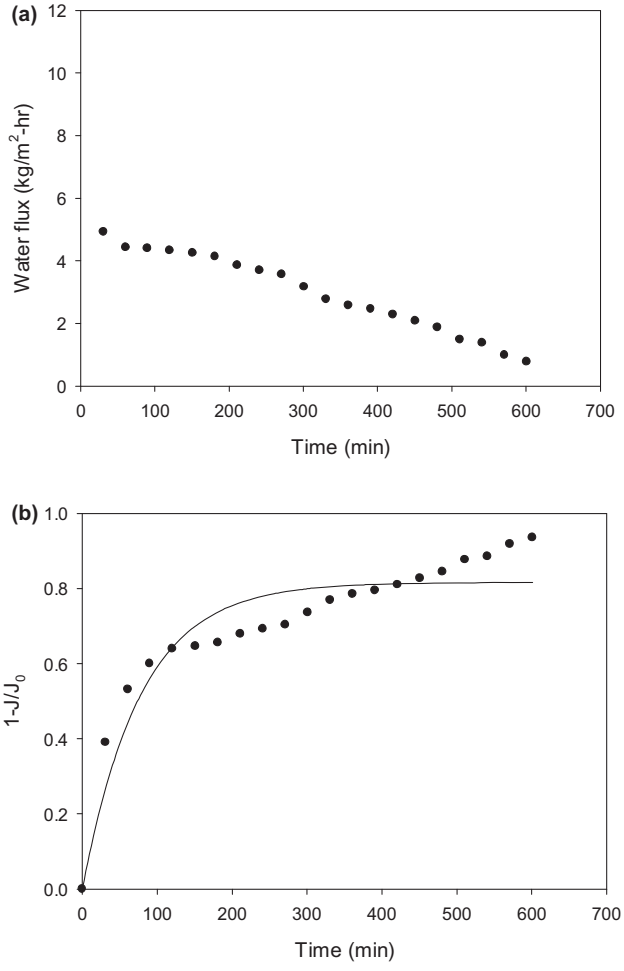

Fig. 8. Changes in flux and pore blockage ratio with time in the presence of antiscalant F during DCMD operation (feed water: NaCl 350 g/L solution; feed temperature: 60˚C; distillate temperature: 20˚C; antiscalant concentration: 10 mg/L) (a) flux and (b) pore blockage ratio (θ).

addition of antiscalant is effective. As expected, the antiscalant C showed the highest values for relative water production and relative flux. The water production was almost two times higher, and the average flux was 1.8 times higher. For the other antiscalants, the relative water production and relative flux range from 1.16 to 1.48 and from 1.13 to 1.42, respectively.

4.4. Morphology of crystals on MD membranes

The SEM analysis was applied to observe the scale formation on the membranes surfaces after the MD operation. Fig. 13(a) shows the image of membrane surface after MD operation without adding any antiscalant. It was found that the entrance of the pores is blocked by the crystals. Although it is not clear from

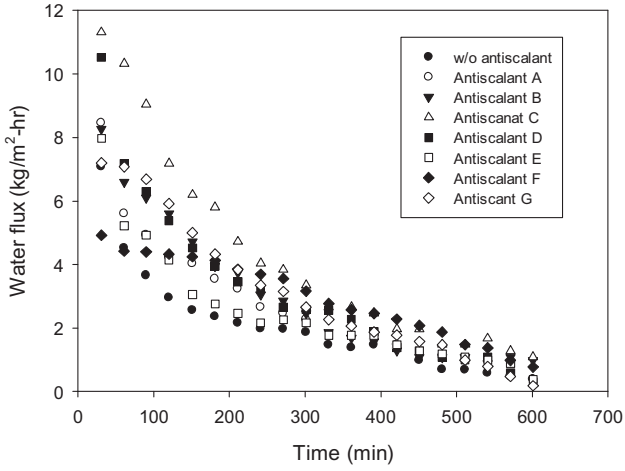

Fig. 9. Comparison of flux behaviors in the presence of antiscalants.

the picture, it is likely that the crystals are also formed inside the pores. The flux after the MD operation was only 3% of the initial flux, implying that most pores are blocked by the crystals.

Fig. 13(b) shows the image of MD membranes when the antiscalant A was used. Unlike the previous case, crystal particles are found on the membrane surface. Moreover, the entrance of the pores seems to be completely blocked by the scales. Similar results are found in Fig. 13(g) where particle layers are found. In these cases, it appears that not only surface blockage but also particle deposition resulted in flux decline.

Fig. 13(d) shows the membrane surface after adding the antiscalant C, which was the most effective to retard scale formation. No blockage of surface pores is observed. Nevertheless, it seems that the internal pores may be blocked by the crystals since flux decline was also observed in this case. Similar result was obtained for the antiscalant G, which is shown in Fig. 13(h). Clearly, the fouling layers with the antiscalant C or G are different from those with the antiscalants A or F.

The other antiscalants, B, D, and E, result in the formation of fouling layer that is similar to that without the use of antiscalant. The blockage of surface pores as well as internal pores could be observed. The foulant layers seem to have intermediate properties between the previous two cases.

4.5. FTIR for antiscalants

As shown in Fig. 14, FTIR was applied to determine major functional groups in the antiscalants. Since the antiscalants are mixtures, only limited information

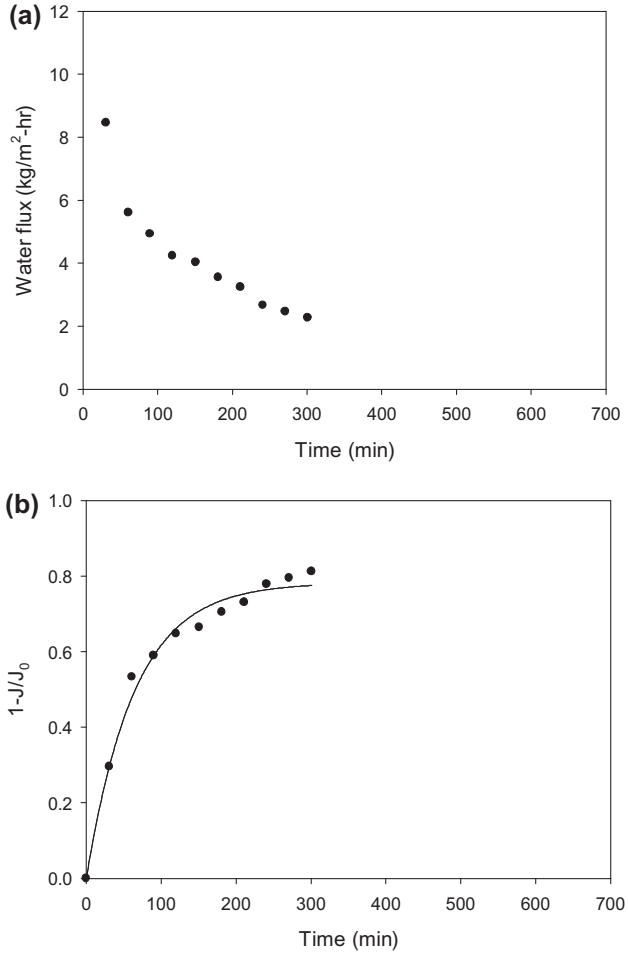

Fig. 10. Changes in flux and pore blockage ratio with time in the presence of antiscalant A during DCMD operation (feed water: NaCl 350 g/L solution; feed temperature: 60˚C; distillate temperature: 20˚C; antiscalant concentration: 10 mg/L) (a) flux and (b) pore blockage ratio (θ).

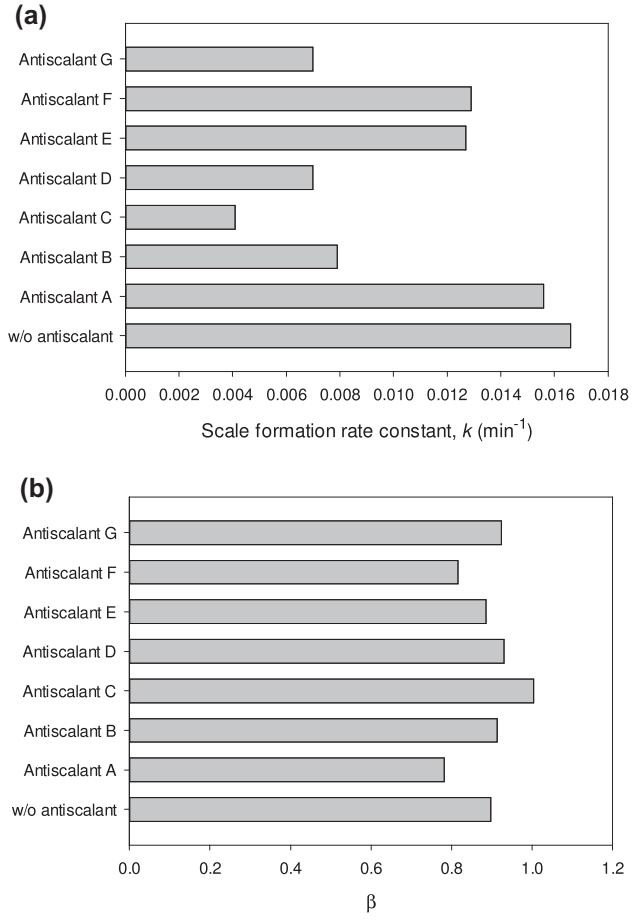

Fig. 11. Comparison of (a) scale formation rate constant (k) and (b) correction factor (β) for various antiscalants in DCMD operation.

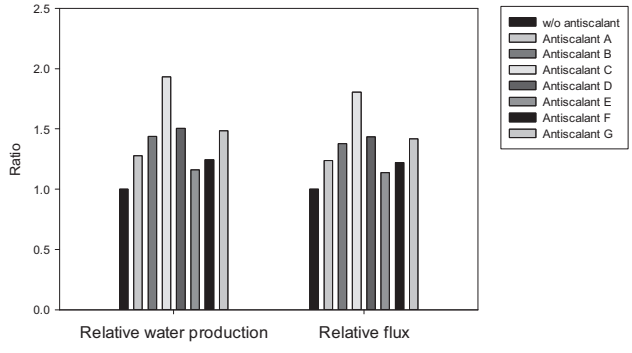

Fig. 12. Comparison of relative water production and relative average flux for various antiscalants in DCMD operation.

is available by the FTIR measurement. Moreover, the detailed compositions of the antiscalants are proprietary. Nevertheless, common functional groups in the antiscalants were identified using the FTIR to interpret their effectiveness. It was confirmed that all antiscalants represent the absorption of N–H (3,400–3,250 cm^{-1}), C–O (1,320–1,000 cm^{-1}), and O–H (3,300–2,500 cm^{-1}). The antiscalant C exhibited the strong and broad band at 3,616 cm^{-1}, which results from free hydroxyl (O–H) functional group. One of the unique peaks in the FTIR spectrum for the antiscalant C appeared at 2,557 cm^{-1}, corresponding to aldehyde functional group. On the other hand, the antiscalant E was the least effective to retard scale formation, which has the major peaks at 3,486 and 1,644 cm^{-1}. Since these peaks are related to N–H bonds, it appears that the amine groups are not effective to control scale formation. Nevertheless, other analytical techniques should be further applied to have a better understanding of the relationship between the effectiveness of antiscalants and their chemical structures.

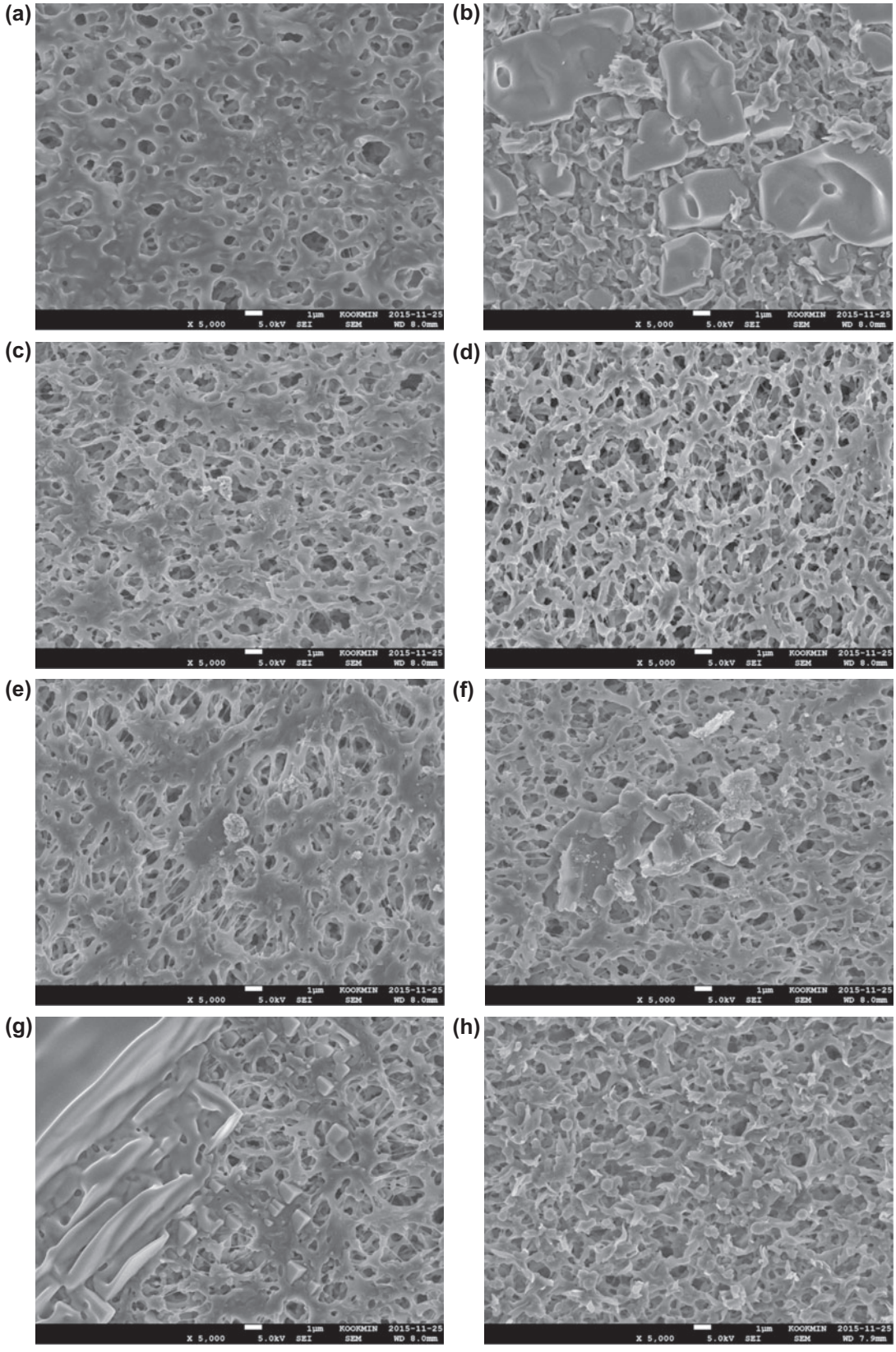

Fig. 13. SEM images after MD experiments (a) without antiscalant, (b) antiscalant A, (c) antiscalant B, (d) antiscalant C, (e) antiscalant D, (f) antiscalant E, (g) antiscalant F, and (h) antiscalant G.

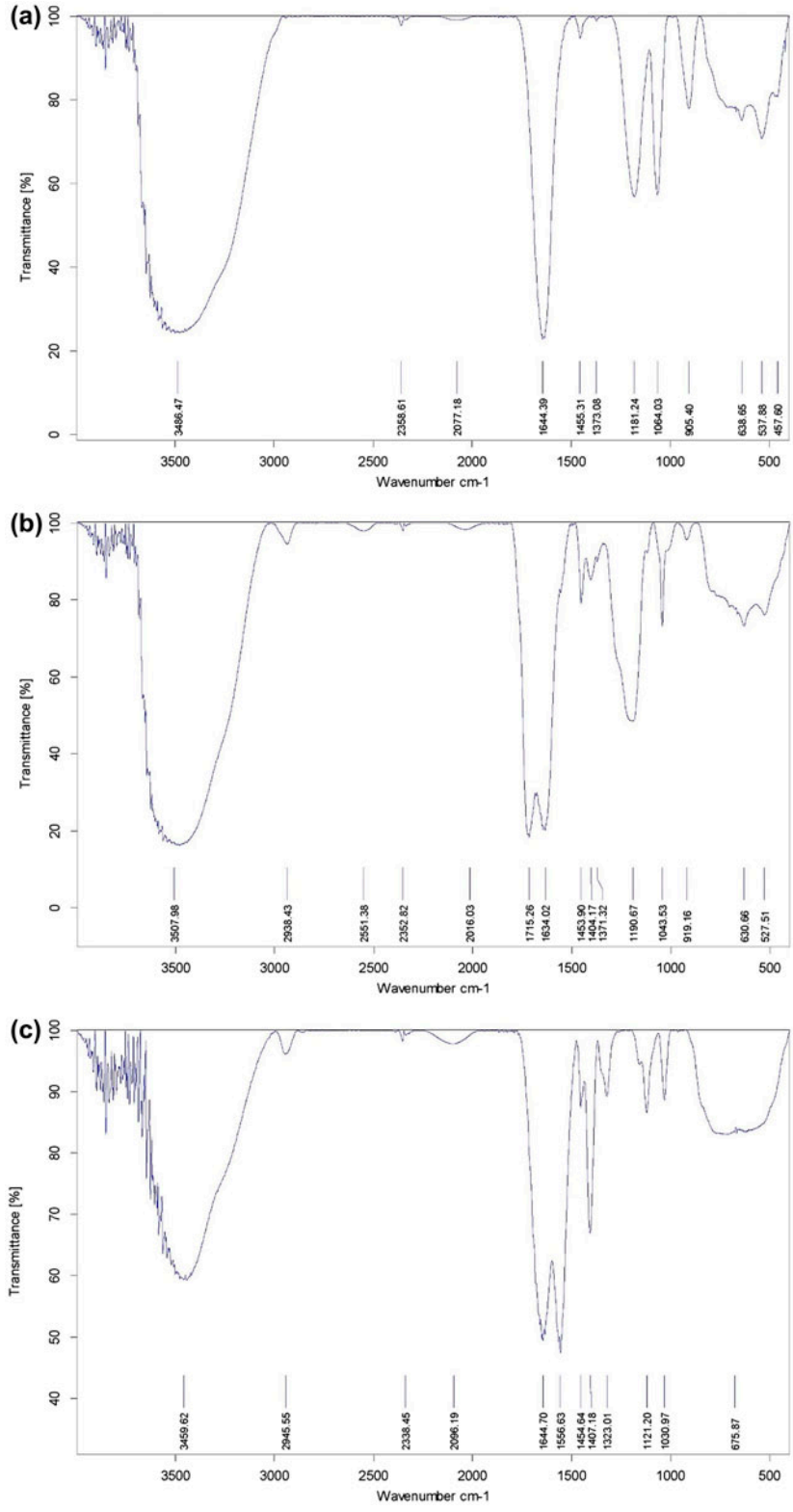

Fig. 14. FTIR spectrum for antiscalants. (a) Antiscalant A, (b) antiscalant B, (c) antiscalant C, (d) antiscalant D, (e) antiscalant E, (f) antiscalant F, and (g) antiscalant G.

5. Conclusions

In this study, the effect of antiscalants on scale formation in MD process was investigated for the treatment of high salinity wastewater including produced water from shale gas extraction. Scale formation in MD system resulted in serious membrane fouling. A simple model based on the blockage mechanism was successfully applied to interpret the experimental results. The effects of scale inhibition were different for different antiscalants. In this study, the antiscalant C was the most effective and the antiscalants A and F were not effective to control scale formation. Using the antiscalants, the apparent rate constants of crystallization are reduced from 0.0166 to 0.0041 min^{-1}. The water production increased up to 1.93 times, and the average flux increased up to 1.80 times. The use of antiscalants affects the fouling mechanisms due to scale formation. With the addition of the antiscalants A and F, surface pore blockage and particle deposition were identified as major fouling mechanisms. On the other hand, internal pore blockage seems to be more important with the addition of the antiscalants C and G. The chemical compositions and structures of the antiscalants seem to be closely related to their effectiveness for scale inhibition.

Acknowledgment

This research was supported by Korea Ministry of Environment as Global Top Project (Project No. GT-14-B-01-003-0).

References

[1] USEIA, Annual Energy Outlook 2012 with Projections to 2035. Vol. DOE/EIA-0383 2012, U.S. Energy Information Administration, U.S. Department of Energy, Washington, DC.
[2] X. Zhang, A.Y. Sun, I.J. Duncan, Shale gas wastewater management under uncertainty, J. Environ. Manage. 165 (2016) 188–198.
[3] G.P. Thiel, E.W. Tow, L.D. Banchik, H.W. Chung, J.H. Lienhard, Energy consumption in desalinating produced water from shale oil and gas extraction, Desalination 366 (2015) 94–112.
[4] B.D. Coday, P. Xu, E.G. Beaudry, J. Herron, K. Lampi, N.T. Hancock, T.Y. Cath, The sweet spot of forward osmosis: Treatment of produced water, drilling wastewater, and other complex and difficult liquid streams, Desalination 333(1) (2014) 23–35.
[5] J. Minier-Matar, A. Hussain, A. Janson, R. Wang, A.G. Fane, S. Adham, Application of forward osmosis for reducing volume of produced/Process water from oil and gas operations, Desalination 376 (2015) 1–8.
[6] A. Alkhudhiri, N. Darwish, N. Hilal, Membrane distillation: A comprehensive review, Desalination 287 (2012) 2–18.
[7] Y. Zhang, Y. Peng, S. Ji, Z. Li, P. Chen, Review of thermal efficiency and heat recycling in membrane distillation processes, Desalination 367 (2015) 223–239.
[8] I. Hitsov, T. Maere, K. De Sitter, C. Dotremont, I. Nopens, Modelling approaches in membrane distillation: A critical review, Sep. Purif. Technol. 142 (2015) 48–64.
[9] L.D. Tijing, Y.C. Woo, J.-S. Choi, S. Lee, S.-H. Kim, H.K. Shon, Fouling and its control in membrane distillation—A review, J. Membr. Sci. 475 (2015) 215–244.
[10] M.A.E.-R. Abu-Zeid, Y. Zhang, H. Dong, L. Zhang, H.-L. Chen, L. Hou, A comprehensive review of vacuum membrane distillation technique, Desalination 356 (2015) 1–14.
[11] H.C. Duong, S. Gray, M. Duke, T.Y. Cath, L.D. Nghiem, Scaling control during membrane distillation of coal seam gas reverse osmosis brine, J. Membr. Sci. 493 (2015) 673–682.
[12] S.A. Ali, I.W. Kazi, F. Rahman, Synthesis and evaluation of phosphate-free antiscalants to control $CaSO_4{\cdot}2H_2O$ scale formation in reverse osmosis desalination plants, Desalination 357 (2015) 36–44.
[13] S. Jamaly, N.N. Darwish, I. Ahmed, S.W. Hasan, A short review on reverse osmosis pretreatment technologies, Desalination 354 (2014) 30–38.
[14] K. Chauhan, R. Kumar, M. Kumar, P. Sharma, G.S. Chauhan, Modified pectin-based polymers as green antiscalants for calcium sulfate scale inhibition, Desalination 305 (2012) 31–37.
[15] C. Wildebrand, H. Glade, S. Will, M. Essig, J. Rieger, K.-H. Büchner, G. Brodt, Effects of process parameters and anti-scalants on scale formation in horizontal tube falling film evaporators, Desalination 204(1–3) (2007) 448–463.
[16] Y.-J. Choi, H. Oh, S. Lee, S.-H. Nam, T.-M. Hwang, Investigation of the filtration characteristics of pilot-scale hollow fiber submerged MF system using cake formation model and artificial neural networks model, Desalination 297 (2012) 20–29.
[17] S. Lee, J. Kim, C.-H. Lee, Analysis of $CaSO_4$ scale formation mechanism in various nanofiltration modules, J. Membr. Sci. 163(1) (1999) 63–74.
[18] S. Lee, C.-H. Lee, Effect of operating conditions on $CaSO_4$ scale formation mechanism in nanofiltration for water softening, Water Res. 34(15) (2000) 3854–3866.
[19] S. Lee, R.M. Lueptow, Control of scale formation in reverse osmosis by membrane rotation, Desalination 155(2) (2003) 131–139.
[20] H.-J. Oh, Y.-K. Choung, S. Lee, J.-S. Choi, T.-M. Hwang, J.H. Kim, Scale formation in reverse osmosis desalination: Model development, Desalination 238(1–3) (2009) 333–346.
[21] J. Koo, S. Lee, J.-S. Choi, T.-M. Hwang, Theoretical analysis of different membrane distillation modules, Desalin. Water Treat. 54(4–5) (2015) 862–870.
[22] J. Koo, J. Han, J. Sohn, S. Lee, T.-M. Hwang, Experimental comparison of direct contact membrane distillation (DCMD) with vacuum membrane distillation (VMD), Desalin. Water Treat. 51(31–33) (2013) 6299–6309.